

## Frequency Dependence of the Vortex-State Resistivity in $\text{YBa}_2\text{Cu}_3\text{O}_{7-\delta}$

Hui Wu,<sup>1</sup> N. P. Ong,<sup>1</sup> and Y. Q. Li<sup>2</sup>

<sup>1</sup>*Joseph Henry Laboratories of Physics, Princeton University, Princeton, New Jersey 08544*

<sup>2</sup>*Department of Materials Science and Engineering, Stevens Institute of Technology, Hoboken, New Jersey 07030*  
(Received 3 May 1993)

Swept-frequency measurements (1–600 MHz) of the vortex resistivity in  $\text{YBa}_2\text{Cu}_3\text{O}_7$  were performed in fields from 0.5 to 8 T. At all fields studied, both the real and imaginary parts of the resistivity display a power-law frequency dependence with exponents  $\alpha_1$  and  $\alpha_2$  that depend only on the reduced field  $h = H/H^*(T)$ . The scaling field  $H^*(T)$  is identified with the critical field for the solid-to-liquid transition. The power-law dependence and the frequency variation of the phase angle are consistent with the model of Fisher, Fisher, and Huse. The field dependence of  $\alpha_1$  and  $\alpha_2$  provides an improved determination of the critical phase angle ( $65.7^\circ$ ) and the dynamic exponent  $z$  (3.7).

PACS numbers: 74.60.Ge, 74.25.Nf, 74.72.Bk

In the presence of a weak oscillating current, vortices in a type II superconductor experience an oscillatory Lorentz force. In the low- $T_c$  superconductors, measurements of the complex response versus frequency ( $\omega$ ) have provided valuable information on the pinning forces. Gittleman and Rosenblum [1] measured the power absorption of the vortex system in PbIn and NbTa films over a wide range of frequencies, and analyzed their data with the equation

$$dx/dt + \omega_{\text{pin}}x = (J\phi_0/\eta)e^{j\omega t} \quad (1)$$

(where  $x$  is the line displacement,  $\eta$  is the damping viscosity,  $\omega_{\text{pin}}$  the pinning frequency,  $J$  the driving current density, and  $\phi_0$  the flux quantum). Similar experiments on the vortex state in the high- $T_c$  superconductors would be of great interest, but few swept-frequency results exist. Olsson, Koch, Eidelloth, and Robertazzi (OKER) [2] measured the impedance of thin-film  $\text{YBa}_2\text{Cu}_3\text{O}_7$  (YBCO) at frequencies up to 500 MHz, but at the single field value 0.55 T. They interpreted their results in terms of the scaling model of Fisher, Fisher, and Huse (FFH) [3]. Whether there exists a critical field (as scaling behavior would suggest) is a central issue in the vortex system in the cuprates [4,5]. The scaling model is based on a diverging correlation length and a slowing down of the characteristic time scale near the transition. Swept-frequency experiments provide a particularly incisive probe of the changing time scale. Thus, it is important to extend OKER's measurements to a much broader range of fields and temperatures. Moreover, it is necessary to clarify the differences between the scaling model and the general class of "mean-field" models exemplified by Eq. (1). Recently, Owliaei, Sridhar, and Talvacchio [6] measured the variation with field of the surface resistance  $R_s$  in thin-film YBCO at the fixed frequency 10 GHz, and found agreement with a model that is a slight generalization of Eq. (1). A sharper distinction between scaling models involving a phase transition and the mean-field models seems necessary.

We have measured the complex resistivity of the vortex state in thin-film YBCO in the frequency range 1–600 MHz in a field that may be varied from 0 to 8 T. The  $c$ -

axis-aligned films (grown epitaxially [7] by metallorganic chemical vapor deposition on  $\text{LaAlO}_3$  substrates) are etched into rectangular strips of area  $9 \times 1 \text{ mm}^2$  and thickness 0.1 to 0.2  $\mu\text{m}$ . The samples, with critical temperatures  $T_c$  of 88–89 K, are placed in the bore of a superconducting magnet, with the field  $\mathbf{H}$  normal to the  $\text{CuO}_2$  planes. Contact pads of resistances under 20 m $\Omega$  are made by evaporating silver film. In our technique [8], the rf signal transmitted through the sample is phase detected by a vector analyzer (Polarad ZPV). The sample impedance  $Z$  is deduced from the phase and amplitude of the transmitted signal. By paying careful attention to impedance matching, we can resolve changes in  $Z$  of 20 m $\Omega$  at 300 MHz. Calibration checks against standard inductors were performed between 1 and 800 MHz. Because  $Z$  spans over 2 decades in the field range of interest, we studied five samples that varied in dc resistance from 10 to 100  $\Omega$  at 100 K. The typical value of  $J = 50 \text{ A/cm}^2$ . A reduction of  $J$  by a factor of 10 does not alter the spectra. Apart from the ability to sweep frequency, an advantage of this technique is that the measured  $Z$  is directly proportional to the complex resistivity, viz.,  $ZA/l = \rho(\omega) = \rho_1(\omega) + i\rho_2(\omega)$  ( $A$  and  $l$  are the film cross section area and length, respectively). Techniques involving microwave resonators [6,9] or induction coils [10] probe only the surface impedance  $R_s$  which must then be converted to the complex resistivity using a model calculation [11].

Before describing the frequency dependence of  $\rho_1(\omega)$  and  $\rho_2(\omega)$ , we discuss how the complex impedance varies with field at fixed frequency (Fig. 1). The dissipative part  $\text{Re}Z$  (proportional to  $\rho_1$ ) increases monotonically with field, but the reactive part  $\text{Im}Z$  (proportional to  $\rho_2$ ) is nonmonotonic. Initially,  $\text{Im}Z$  increases linearly with  $B$ , reflecting the increase in vortex density. However, at 3.0 T (arrow) it deviates upwards, and attains a maximum near 5 T. Further increase in field causes  $\text{Im}Z$  to drop rapidly. With measurements limited to a single frequency, Eq. (1) may be made to agree with Fig. 1, if we assume that the field reduces  $\omega_{\text{pin}}$ , so that the system crosses over from the inductive ( $\omega \ll \omega_{\text{pin}}$ ) to the dissipative regime ( $\omega \gg \omega_{\text{pin}}$ ) [6]. However, such a simple sce-

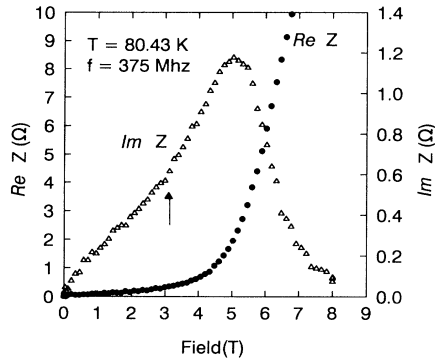


FIG. 1. Variation of  $\text{Re}Z(\omega) = \rho_1 l/A$  and  $\text{Im}Z(\omega) = \rho_2 l/A$  in thin-film YBCO with magnetic field, at the fixed frequency 375 MHz. The break in slope in  $\text{Im}Z$  near 3.0 T (arrow) coincides with the critical field  $H^*$  (see text).  $\text{Im}Z$  continues to increase until 5 T, beyond which it decreases rapidly to zero.

nario is actually incompatible with the swept-frequency results to be discussed next. The swept-frequency experiments reveal a universal pattern in the way the field alters the spectra of  $\rho_1$  and  $\rho_2$  and (especially) the phase angle. These results highlight an important difference between the scaling model and mean-field models such as Eq. (1).

In general, both  $\text{Re}Z$  and  $\text{Im}Z$  display power-law behavior within our frequency window. In the main panel of Fig. 2 we have plotted in log-log scale  $\text{Re}Z$  (four uppermost curves) and  $\text{Im}Z$  (four lowest curves) versus  $\omega$  for selected values of  $H$ , with the temperature  $T$  fixed at 80.9 K. At the three lowest fields,  $\rho_1$  fits well to a strict power law,  $\omega^{\alpha_1}$ . (Hereafter, we use  $\rho_1$  and  $\rho_2$  in place of  $\text{Re}Z$  and  $\text{Im}Z$ , respectively.) The fits (solid lines) give an exponent  $\alpha_1$  that decreases with field ( $\alpha_1 = 0.95, 0.835,$  and  $0.76$  at 1.0, 2.4, and 2.82 T, respectively). Similarly, the reactive component  $\rho_2$  ( $\sim \text{Im}Z$ ) follows a strict power law  $\omega^{\alpha_2}$ . In the same field range,  $\alpha_2$  decreases from 0.80 to 0.73. When the field exceeds a critical value (very close to 2.82 T at this temperature) the dc resistivity  $\rho_{xx} \equiv \rho_1(0)$  increases rapidly with field. In the liquid state (for example the curve at 4.03 T)  $\rho_1$  may be fitted to  $\rho_1(\omega) = \rho_{xx} + A\omega^{\alpha_1}$ , provided  $\rho_{xx}$  is not too large [12]. The strict power-law fit, however, remains valid for  $\rho_2$  deep into the liquid state. To summarize, we replot  $\rho_1$  in linear-linear scale in the inset. At 1 T, the curve of  $\rho_1$  vs  $\omega$  is almost linear ( $\alpha_1 = 0.95$ ), but at 2.82 T (close to the solid-liquid transition line), the curve acquires significant *negative* curvature ( $\alpha_1 = 0.76$ ). In the liquid state at 4.03 T,  $\rho_{xx}$  is finite ( $\text{Re}Z \sim 0.1 \Omega$  at  $\omega = 0$ ), but remains a small fraction of the total dispersion.

The striking power-law dependence with fractional exponents is observed in all samples over the range of fields (0.5–8 T) and temperatures (80–86 K) investigated. We now analyze their field dependence. At each temperature,  $\alpha_1$  is close to 1.0 at low fields, but falls steeply to values less than 0.4 with increasing field. In contrast,  $\alpha_2$  varies slowly from 0.8 to 0.65. Thus, their trajectories

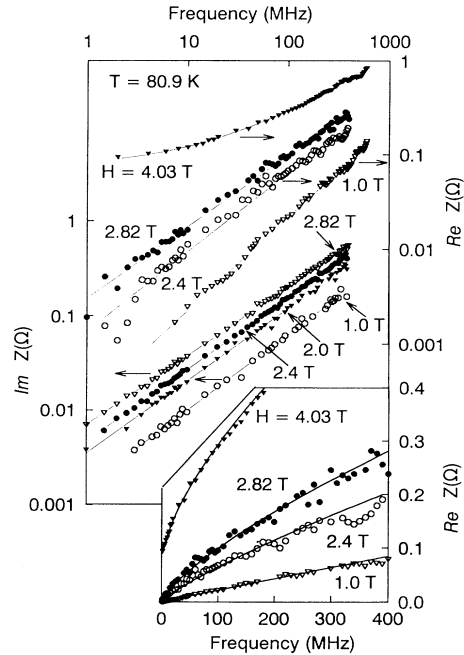


FIG. 2. Main panel: Log-log plot of  $\text{Re}Z = \rho_1 l/A$  (four uppermost curves) and  $\text{Im}Z = \rho_2 l/A$  (four lower curves) versus frequency  $\omega$  at the fields indicated. Solid lines are fits to power-law behavior. At 1 T, the exponent  $\alpha_1$  (of  $\text{Re}Z$  vs  $\omega$ ) equals 0.95, whereas  $\alpha_2(\text{Im}Z) = 0.80$ . However, they become almost equal ( $\alpha_1 = 0.76$  and  $\alpha_2 = 0.73$ ) when the field (2.82 T) is close to the transition field for this temperature (80.9 K). All curves are from sample A, except the uppermost curve at 4.03 T (from sample B). An  $\omega$ -independent contact resistance of 20 m $\Omega$  has been subtracted from each curve. In the inset, the *same* data set for  $\text{Re}Z$  is replotted in linear scale to highlight the negative curvature at 2.4, 2.82, and 4.03 T.

must intersect at some field  $H^*(T)$  that depends only on  $T$ . Remarkably, we find that  $\alpha_1$  and  $\alpha_2$  collapse onto two universal curves if we plot them against the reduced field  $h = H/H^*(T)$  (see Fig. 3) [see Ref. 13]. Thus, within our resolution, the scaling field is also the field  $H^*$  at which  $\alpha_1 = \alpha_2$ . The universal behavior shown in Fig. 3 provides a surprisingly simple description of the vortex response in the field and temperature range studied, and justifies the field-scaling procedure. We identify  $H^*$  as the critical field separating the solid from the liquid state. Moreover, the near coincidence of  $H^*(T)$  to the critical field  $H_g$  for the “vortex glass-to-liquid” transition [4,5] in the phase diagram of YBCO (inset in Fig. 3) suggests that  $H^*$  is identical with  $H_g$ .

The universal curves show that  $\alpha_2 - \alpha_1$  is negative when  $h < 1$  and positive when  $h > 1$ . This change in sign has interesting implications for the phase angle

$$\tan\phi(\omega) = \rho_2/\rho_1 \sim \omega^{(\alpha_2 - \alpha_1)}, \quad 0 < h < \sim 1.5. \quad (2)$$

Equation (2) implies that  $\tan\phi$  increases (decreases) with  $\omega$  when  $\alpha_2 - \alpha_1$  is positive (negative), and is frequency in-

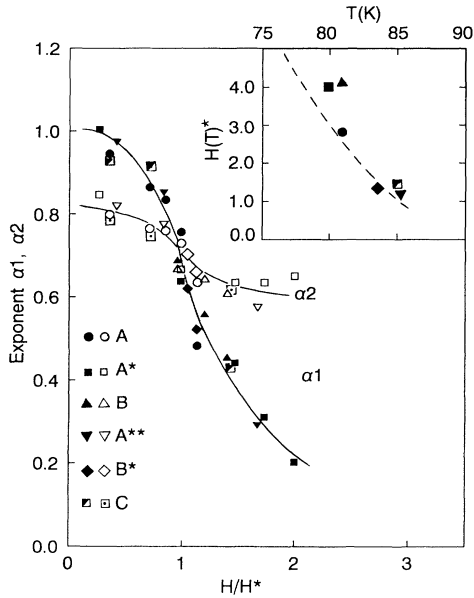


FIG. 3. The variation of the exponents  $\alpha_1$  (solid symbols) and  $\alpha_2$  (open symbols) versus the reduced field  $h$  in three samples (A, B, and C). See Ref. [13] for details. Within our scatter,  $\alpha_1$  and  $\alpha_2$  fall on two universal curves. Lines are guides to the eye. At the intersection ( $h=1$ ) the critical value  $\alpha_c=0.73\pm 0.03$ . The temperatures (in K) are 80.9 (A), 80.0 (A\*), 85.3 (A\*\*), 81.1 (B), 83.6 (B\*), and 85.1 (C). In the inset,  $H^*(T)$  is compared with the transition line (broken line) reported by Koch *et al.* [4] and by Gammel, Schneemeyer, and Bishop [5].

dependent at  $h=1$ . This overall trend is illustrated in Fig. 4 which plots  $\tan\phi$  vs  $\omega$  for fields on either side of the transition. In the "solid" phase (curves at  $h=0.4, 0.71$ , and  $0.85$ ),  $\tan\phi(\omega)$  is observed to decrease weakly with increasing  $\omega$ . We recall that a phase angle that decreases with increasing  $\omega$  is characteristic of a pinned vortex (inductive at small  $\omega$ , but dissipative at large  $\omega$ ). For instance, Eq. (1) predicts that  $\tan\phi(\omega)=\omega_{\text{pin}}/\omega$ , i.e.,  $\phi$  approaches zero as  $1/\omega$ . However, in YBCO, the smallness of the parameter  $|\alpha_2-\alpha_1|$  implies that the decrease in  $\tan\phi(\omega)$  is *much slower* ( $\omega^{-0.18}$ ) at  $h=0.4$  to  $\sim\log\omega$  as  $h\rightarrow 1$ ). Moreover, in the limit of high frequencies,  $\tan\phi$  approaches the finite value  $\tan\phi_c\sim 2.1\pm 0.1$ , rather than zero. It is interesting that even in the "solid" phase, there exist qualitative disagreements with the mean-field models.

We now compare our findings with the scaling model of FFH. Dorsey [14] has shown that at the critical point the conductivity  $\sigma(\omega)$  equals  $(-i\omega)^{\alpha_c}$ , i.e.,  $\alpha_1=\alpha_2=\alpha_c$ . From this, Dorsey predicts that the critical phase angle has the  $\omega$ -independent value  $\phi_c=\alpha_c\pi/2=\pi/2[1-(d-2)/z]$  (the dynamic exponent  $z$  relates the time scale  $\tau$  to the coherence length  $\xi$  by  $\tau\sim\xi^z$ ). Identifying the intersection point in Fig. 3 with the critical point, we obtain  $\alpha_c=0.73\pm 0.03$ , from which

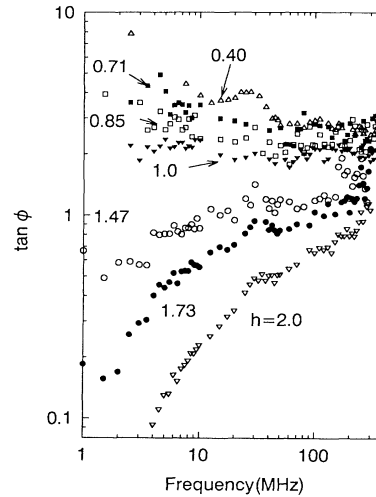


FIG. 4. The frequency dependence of the  $\tan\phi$  in log-log plot for reduced fields (as indicated) above and below the critical value. At the critical value  $h=1$ ;  $\tan\phi$  has the  $\omega$ -independent value  $2.1\pm 0.1$ . Curves at  $h=0.71, 0.85$ , and  $1.0$  are from sample A, whereas curves at  $h=1.47, 1.73$ , and  $2.0$  are from sample B. At large fields ( $h=1.73, 2.0$ ), where  $\rho_{xx}$  is significant, the contribution of  $\rho_{xx}$  is included in computing  $\tan\phi$ .

$$\phi_c=65.7^\circ\pm 2^\circ \text{ and } z=3.70\pm 0.46. \quad (3)$$

As discussed above, the phase angle changes with  $\omega$  both above and below the critical field, but at  $h=1$  it remains independent of frequency (from 2 to 600 MHz) at the value  $\tan\phi_c=2.1\pm 0.1$  (Fig. 4). Our values for  $\phi_c$  and  $z$  are significantly smaller than OKER's [2]. In their experiment, OKER determined the transition temperature  $T_g$  (at the field 0.55 T) by measuring the dc  $I$ - $V$  curves. At  $T_g$ , they observe that the amplitude  $|Z|$  varies as  $\omega^{0.83}$ . Also, the phase angle at  $T_g$  is shown to be  $\omega$  independent over about 1 decade in frequency. From their value of  $\phi_c$  ( $74^\circ$ ) OKER obtain  $z=5.6$ , which is comparable with  $z=5.2$  deduced from the dc  $I$ - $V$  curves. (The disagreement seems to lie outside our measurement uncertainty. To get OKER's value  $z=5.6$ , the two lines in Fig. 3 would have to intersect at  $\alpha_c=0.82$ , which is outside our error bars. Also, a critical value of  $\tan\phi$  as large as  $\tan 74^\circ=3.49$  seems incompatible with the data in Fig. 4.) Aside from the numerical difference, the two experiments are qualitatively consistent.

Figure 3 shows that in the liquid state ( $h>1$ ),  $\alpha_1$  decreases rapidly whereas  $\alpha_2$  remains near the value 0.64. Therefore, the phase angle must increase with frequency as a power law [Eq. (2)]. This is illustrated by the curve in Fig. 4 at the reduced field 1.47, which shows  $\tan\phi$  approaching the critical value from below as  $\omega$  increases. At higher fields ( $h=1.73$  and  $2.0$ ) the phase angle increases even faster with frequency. However, there is now noticeable deviation from strict power-law behavior [Eq. (2)]. This reflects the increasing dominance of  $\rho_{xx}$  over the dispersive part of  $\rho_1$  which spoils the power-law

description [12].

The striking pattern that emerges from Fig. 4 is that the frequency dependence of  $\tan\phi$  changes from a decreasing function to an increasing function of  $\omega$  as the reduced field exceeds 1. As noted above, models such as Eq. (1) and those used in Refs. [6] and [11] would predict a phase angle that monotonically approaches zero at large  $\omega$ . The observed phase-angle behavior seems difficult to reconcile with such mean-field models. In contrast, it is consistent with a central prediction of the scaling model of FFH. Near the critical temperature, the phase angle is an odd function of its argument that may be written [3,14] as (using the reduced temperature  $t = T/T_c$  instead of  $h$ )

$$\phi(t, \omega) = P_\sigma(x), \quad x = (t-1)\omega^{-1/z_v}. \quad (4)$$

Above the transition ( $x > 0$ ),  $P_\sigma$  decreases from the critical value  $\alpha_c\pi/2$  to zero as  $x \rightarrow +\infty$ . By rewriting the argument as  $x = (1/\tau\omega)^{1/z_v}$ , we see that  $P_\sigma$  depends (up to a sign) only on the ratio of the ac period to the characteristic time  $\tau$  of the system. Increasing  $\omega$  at fixed  $\tau$  has the same effect as increasing  $\tau$  at fixed  $\omega$ . Thus, above the critical temperature, increasing the frequency mimics the effect of moving the system closer to the transition, whence  $\tan\phi$  increases monotonically with frequency to its critical value  $\tan\phi_c$ . Conversely, below  $T_c$ ,  $\tan\phi$  decreases to its critical value with increasing frequency. These predictions are consistent with the results in Fig. 4 if we replace  $t$  with the reduced field ( $h-1$ ). The phase angle decreases with frequency when the vortex is in the "solid" state ( $h < 1$ ), whereas it has the opposite trend in the "liquid" state ( $h > 1$ ).

In conclusion, we find that between 1 and 600 MHz the complex resistivity in the vortex state of YBCO displays power-law frequency dependence with fractional exponents  $\alpha_1$  and  $\alpha_2$ . From the field dependence of the exponents, we obtain a scaling behavior that is consistent with predictions derived from the vortex-glass model. In particular, at the critical field, the value  $\alpha_c = 0.73$  determines the critical phase angle ( $65.7^\circ$ ) and the dynamic exponent  $z$  (3.7). Away from the critical line, the phase angle  $\phi$  is observed to decrease with increasing frequency in the solid state, but to increase with  $\omega$  in the liquid state, in agreement with the scaling model of FFH. Such unusual behavior is incompatible with models such as Eq. (1) that do not incorporate a diverging scaling length.

We thank David Huse for several enlightening discussions. Research performed at Princeton University was supported by the Office of Naval Research (Contract No. N00014-90-J-1013.P2) and the Seaver Institute. Y.Q.L. is supported by Contract No. N00014-91-C-0231 from the Defense Advanced Research Projects Administration.

- [1] J. I. Gittleman and B. Rosenblum, Phys. Rev. Lett. **16**, 734 (1966).
- [2] H. K. Olsson, R. H. Koch, W. Eidelloth, and R. P. Robertazzi, Phys. Rev. Lett. **66**, 2661 (1991).
- [3] M. P. A. Fisher, Phys. Rev. Lett. **62**, 1415 (1989); Daniel S. Fisher, Matthew P. A. Fisher, and David A. Huse, Phys. Rev. B **43**, 130 (1991).
- [4] R. H. Koch, V. Foglietti, W. J. Gallagher, G. Koren, A. Gupta, and M. P. A. Fisher, Phys. Rev. Lett. **63**, 1511 (1989).
- [5] P. L. Gammel, L. F. Schneemeyer, and D. J. Bishop, Phys. Rev. Lett. **66**, 953 (1991).
- [6] J. Owliaei, S. Sridhar, and J. Talvacchio, Phys. Rev. Lett. **69**, 3366 (1992).
- [7] Y. Q. Li, J. Zhao, C. S. Chern, W. Hang, G. A. Kulesha, P. Lu, B. Gallois, P. Norris, B. Kear, and F. Cosandey, Appl. Phys. Lett. **58**, 648 (1991).
- [8] A major difficulty is the elimination of end reflections which set up line resonances in the long (1.5 m) probe. The sample forms a shunt between the inner and outer conductors. Insertion of a matched resistor directly upstream from the sample eliminates most of the reflected signal from the sample. Residual reflections off the ends of the cables are minimized by using precision matched loads and directional couplers. The transmitted wave is given by  $V_T(\omega) = e^{-jk(l_1+l_2)}\Gamma_T[1+g]V_0$ , where  $V_0$  is the incident amplitude,  $Z_0$  the line impedance, and  $l_1, l_2$  are the cable lengths. The transmission coefficient  $\Gamma_T$  equals  $2Z/(2Z_0+3Z)$ . The term  $g = e^{-j2kl_2}[\gamma_1Z + \gamma_2(Z - 2Z_0)]/[2Z_0+3Z]$  corrects for residual end reflections. Hui Wu and N. P. Ong (to be published).
- [9] D. C. Morgan, K. Zhang, D. A. Bonn, R. Liang, W. N. Hardy, A. J. Berlinsky, and C. Kallin, Bull. Am. Phys. Soc. **38**, 71 (1993).
- [10] D. S. Reed, N. C. Yeh, W. Jiang, T. A. Tombrello, A. P. Rice, U. Kriplani, R. Brain, E. S. Daniel, and F. Holtzberg, Bull. Am. Phys. Soc. **38**, 70 (1993).
- [11] M. W. Coffey and J. R. Clem, Phys. Rev. Lett. **67**, 386 (1991).
- [12] In the liquid state ( $h > 1$ ) our finite frequency span allows  $\alpha_1$  to be determined reliably only if  $\rho_{xx} < 15\%$  of  $\rho_1(\omega = 600 \text{ MHz})$  (see the curve at 4.03 T in Fig. 2). For  $h > 1.5$ , the fit  $\rho_1(\omega) = \rho_{xx} + A\omega^{\alpha_1}$  becomes increasingly unsatisfactory, although  $\rho_2 \sim \omega^{\alpha_2}$  remains valid.
- [13] We explain the scaling procedure in Fig. 3. For a data set in which the field range is wide enough for  $\alpha_2 - \alpha_1$  to change sign (sets A, A\*, A\*\* and C), we first plot  $\alpha_1$  and  $\alpha_2$  against  $H$ . By interpolation,  $H^*$  is reliably determined as the field at which  $\alpha_2 - \alpha_1 = 0$ . Knowing  $H^*(T)$  allows us to replot the exponents versus  $h = H/H^*$  in Fig. 3. The sixteen pairs of points in the four sets suffice to determine the two curves. For a set with smaller field range (B or B\*), we adjust  $H^*$  by trial and error until all the data in the set *simultaneously* fall on the two curves.
- [14] Alan T. Dorsey, Phys. Rev. B **43**, 7575 (1991).